Fluctuation Effects in Ternary AB + A + B Polymeric Emulsions

Dominik Düchs,[†] Venkat Ganesan,[‡] Glenn H. Fredrickson,[§] and Friederike Schmid*,[†]

Fakultät für Physik, Universität Bielefeld, Universitätsstrasse 25, 33615 Bielefeld, Germany, Department of Chemical Engineering, University of Texas at Austin, Austin, Texas 78712, and Departments of Chemical Engineering and Materials, University of California, Santa Barbara, California 93106

Received April 7, 2003; Revised Manuscript Received September 8, 2003

ABSTRACT: We present a Monte Carlo approach to incorporating the effect of thermal fluctuations in field theories of polymeric fluids. This method is applied to a field-theoretic model of a ternary blend of AB diblock copolymers with A and B homopolymers. We find a shift in the line of order−disorder transitions from their mean-field values, as well as strong signatures of the existence of a bicontinuous microemulsion phase in the vicinity of the mean-field Lifshitz critical point. This is in qualitative agreement with a recent series of experiments conducted with various three-dimensional realizations of this model system. Further, we also compare our results and the performance of the presently proposed simulation method to that of an alternative method involving the integration of complex Langevin dynamical equations.

I. Introduction

A straightforward approach to improving the properties of polymeric materials, such as their stiffness, conductivity, toughness, is to blend two homopolymer species (A and B) into a single melt.[1,3−5] However, in most cases, weak segregation tendencies between A and B monomers[6] usually cause such a direct blend to macroscopically phase separate below a critical temperature or, equivalently, above a critical strength of interaction.[2] Such phase separation often leads to poor quality materials with nonreproducible morphologies and weak interfaces. To circumvent this problem, one typically introduces compatibilizers into the system, most commonly multicomponent polymers like block, graft, or random copolymers.[7] Such compatibilizers preferentially segregate toward the interfaces between the bulk A and B domains, thereby lowering interfacial tensions, stabilizing the formation of complex morphologies,[8−11] and strengthening interfaces.[12−15] The compatibilizers so added are usually the most expensive component of a blend, and consequently, theoretical studies of the phase behavior of such blends possess important ramifications in rendering such industrial applications more economically feasible.

Here we examine the phase behavior of a ternary blend of symmetric A and B homopolymers with an added AB block copolymer as a compatiblizer. Specifically, we consider symmetric diblock copolymers wherein the volume fractions of the two different blocks in the copolymer are identical. Moreover, the ratio of the homopolymer and copolymer lengths is denoted as α and is chosen as $\alpha = 0.2$. This is largely motivated by a recent series of experiments by Bates et al.[16−19] on various realizations of the ternary AB + A + B system with $\alpha \approx 0.2$. A combination of neutron scattering, dynamical mechanical spectroscopy, and transmission electron microscopy (TEM) was used to examine the phase behavior. An example of an experimental phase diagram is shown in Figure 1. It will be discussed in detail further below.

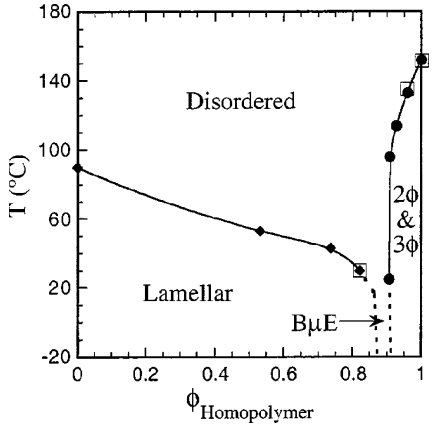

Figure 1. Experimental phase diagram[19] of a PDMS−PEE/PDMS/PEE blend with $\alpha \approx 0.2$. Reproduced with permission from ref 19. Copyright 1999 The Royal Society of Chemistry.

Theoretically, one of the most established approaches to studying such polymer blends is the self-consistent field theory (SCFT), first introduced by Edwards[20] and Helfand[21] and later used, among others, by Scheutjens and Fleer,[22,23] Noolandi et al.,[24] and Matsen et al.[10] In implementing SCFT,[25] one typically chooses (a) a model for the polymers and (b) a model for the interactions. Most researches adopt the Gaussian chain model, wherein the polymers are represented as continuous paths in space.[26] It models polymers as being perfectly flexible; i.e., there exists no free energy penalty for bending. Instead, it features a penalty for stretching. (In contexts where the local rigidity or orientation effects are important, the wormlike chain model[27] serves as a popular alternative.) Such a molecular model for the polymers is typically supplemented by a model for the interactions between unlike polymers, which is usually chosen as an incompressibility constraint plus a generalization of the Flory−Huggins local contact interaction term, whose strength is governed by the product of the segregation parameter, χ, and the polymerization index, N.

[†] Universität Bielefeld.
[‡] University of Texas at Austin.
[§] University of California, Santa Barbara.

10.1021/ma030201y CCC: $25.00
Published on Web 11/04/2003

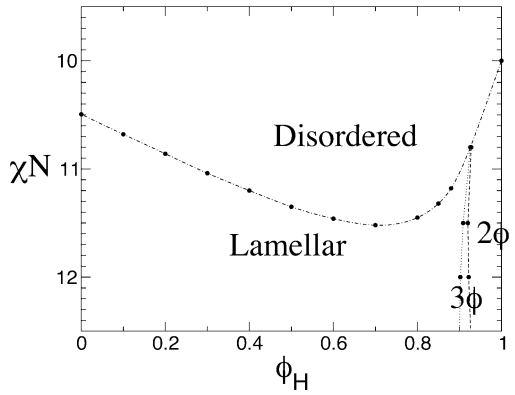

Figure 2. Mean-field phase diagram for a ternary AB + A + B blend with $\alpha = 0.2$, as obtained from a Fourier space implementation of SCFT. 2ϕ denotes a region of two-phase coexistence between an A-rich and a B-rich phase and 3ϕ one of three-phase coexistence between an A-rich, a B-rich, and a lamellar phase. See text for more explanation.

We have implemented SCFT for the above model of polymers, and investigated the phase behavior of the ternary A + B + AB blend. Figure 2 displays the resulting mean-field phase diagram in the coordinates of homopolymer volume fraction ϕ_H and segregation strength χN. Note that the phase diagram shown is a slice along the "isopleth" where the two homopolymers are blended in equal proportions. It can be observed that on the copolymer-rich side of the diagram shown in Figure 2, a line of order−disorder transitions (ODT) separates the disordered region (which occurs at low interaction strengths, χN) from a periodically ordered (i.e., lamellar) phase at higher χN. For pure copolymers ($\phi_H = 0$), this transition is predicted within mean-field theory to occur at $\chi N = 10.495$, and the line of ODTs, often referred to as the Leibler line, represents second-order transitions. On the homopolymer-rich side of the diagram, we find a line of second-order transitions from a disordered phase at low χN to a region of two coexisting homogeneous liquid phases at high χN. For the pure homopolymer system ($\phi_H = 1$), the upper critical consolute point is found by mean-field Flory−Huggins theory to be at $\alpha\chi N = 2$. This line of continuous transitions is referred to as Scott line.[28] The point where the Leibler and Scott lines meet is found, again within mean-field theory, to be an isotropic Lifshitz critical point (LP),[29] which in the case of $\alpha = 1$ becomes a Lifshitz tricritical point (LTP) according to Broseta and Fredrickson[30] and is predicted to occur at a total homopolymer fraction of $\phi_L = 1/(1 + 2\alpha^2)$ and an incompatibility of $(\chi N)_L = 2(1 + 2\alpha^2)/\alpha$. The separation into microphases (i.e., lamellae) observed along the Leibler line displays a steady increase in the lamellar periodicity until it finally diverges at the LP, giving rise to macrophase separation along the Scott line. Below the LP in the ordered regime, the system undergoes a first-order transition from the lamellar (L) to the two-phase (A + B) region along the axis of homopolymer concentration, ϕ_H. Contrary to a previous publication[18] in which this transition was displayed as continuous, a careful reexamination of the mean-field theory reveals that it is indeed first-order with a three-phase (L + A + B) coexistence region reaching all the way up to the LP for any α. This is further corroborated by recent results of Naughton and Matsen.[31]

The mean-field phase diagram displayed in Figure 2 differs substantially from the experimental phase diagram, shown in Figure 1. In the experiments, the LP was destroyed by fluctuations, giving rise to a bicontinuous microemulsion phase in its vicinity. At lower temperature T, the L and A + B phases were conjectured to be separated by a narrow channel of this microemulsion phase stretching down from the Lifshitz region, while the Leibler and Scott lines were shifted from their mean-field locations to lower temperatures (i.e., higher χN, which is proportional to $1/T$). Experimental results are consistent with the picture that as the lamellar periodicity increases along the ϕ_H axis, the persistence length of composition fluctuations along the microdomain boundaries decreases until at some point the two become comparable in size and the lamellae begin to rupture, forming a bicontinuous structure.

The experimental results discussed above, while in contradiction to the mean-field SCFT calculations, are not entirely surprising when viewed in the context of theoretical studies pertaining to the effect of fluctuations on the mean-field phase diagrams. Indeed, even in the context of the pure diblock copolymer (i.e., $\phi_H = 0$), Leibler[32] speculated that the order−disorder transition (predicted to be second order within the mean-field theory) would become a weakly first-order transition when the effects of fluctuations are accounted for. Such a reasoning was confirmed quantitatively by Fredrickson and Helfand,[33] who extended an earlier analysis by Brazovskii[34] to show that fluctuations change the order of the transition and also shift the transition to higher incompatibilities, χN. Further, they quantified such shifts in terms of a parameter that depends on the polymer density (or, equivalently in the context of a polymer melt, their molecular mass N). This parameter, denoted generically as C in this text, acts as a Ginzburg parameter,[35] and in the limit $C \rightarrow \infty$, the mean-field solution is recovered.

The present study is motivated by the hypothesis that the fluctuation effects not accounted for within SCFT are responsible for the discrepancies noted between the experimental results and the theoretical predictions for the ternary-blend phase behavior. As a partial confirmation of our hypothesis, the experimental phase diagrams (Figure 1) of Bates and co-workers deviate most clearly from the mean-field diagram for the PEE/PDMS/PEE−PDMS system, in situations where the molecular weights were much lower than in the other systems (i.e., where the C parameter is small). This article presents a theoretical examination of the effect of thermal fluctuations upon the phase behavior of ternary blends. Our primary goal is to understand and quantify the shift in both the Leibler and Scott lines and to examine the formation of the microemulsion phases in such systems. Bicontinuous structures such as the ones observed in the above experiments are particularly interesting from an application point of view in that they are able to impart many useful properties on polymer alloys. For example, if one blend component is conducting or gas-permeable, these properties will be passed on to the entire alloy. Also, mechanical properties such as the strain at break and the toughness index have been observed to exhibit maxima with co-continuous structures.[36]

Previous simulation studies of fluctuation effects in ternary diblock copolymer/homopolymer blends,[37−41] have mostly focused on the $\alpha = 1$ case. Within a lattice polymer model, Müller and Schick[37] have investigated the phase diagram of a corresponding symmetrical A +

B + AB blend. According to their results, the disordered phase extends to higher χN than predicted by the mean field theory, and the LTP is replaced by a regular tricritical point. Because of finite size effects, the transition to the lamellar phase could not be localized quantitatively.

Particle-based models have the disadvantage that one is restricted to studying relatively short polymers. This motivates the use of field theories in simulations. Kielhorn and Muthukumar[41] have studied the phase separation dynamics in the vicinity of the LTP within a Ginzburg−Landau free energy functional, which they derived from the Edwards model[20] within the random phase approximation (RPA), in the spirit of the theories for pure diblock copolymer systems mentioned earlier.[32,33] Naively, one should expect that such a description is adequate in the weak segregation limit, where the correlation length for composition fluctuations is large. However, Kudlay and Stepanow[42] have recently questioned this assumption. They pointed out that the fluctuations in RPA-derived Hamiltonians have significant short wavelength contributions which cannot be eliminated by renormalization and may lead to unphysical predictions.

In this work, we propose an alternative field-theoretic approach which rests directly on the Edwards model, without resorting to the additional RPA approximation. The partition function is evaluated with a Monte Carlo algorithm. A related algorithm, the complex Langevin method, has been presented recently by two of us.[43−45] Here we study two-dimensional ternary blends at $\alpha = 0.2$ with both methods and compare the results.

The remainder of this article is organized as follows. In section II, we outline the field-theoretic formulation of our model. The simulation method is presented in section III. In section IV, we present and discuss our results before we conclude in section V with a summary and an outlook on future work.

II. The Field-Theoretic Model

In this section, we present a field-theoretic model for the system under consideration. To this effect, we consider a mixture of n_A homopolymers of type A, n_B homopolymers of type B, and n_{AB} symmetric block copolymers in a volume V. The polymerization index of the copolymer is denoted N, and the corresponding quantities for the homopolymers are denoted $N_A = N_B = \alpha N$. All chains are assumed to be monodisperse. We consider the case of symmetric copolymers, where the fraction of A monomers in the copolymer is $f = {}^1/_2$. We restrict our attention to the concentration isopleth, where the homopolymers have equal volume fractions $\phi_{HA} = \phi_{HB} = \phi_H/2$. The monomeric volumes of both A and B segments are assumed to be identically equal to $1/\rho_0$. In this notation, the incompressibility constraint requires

$$n_A = n_B = \frac{\phi_H \rho_0 V}{2\alpha N}; \quad n_{AB} = (1 - \phi_H)\frac{\rho_0 V}{N} \tag{1}$$

where V denotes the volume of the system. In the Gaussian chain model, the segments are assumed to be perfectly flexible and are assigned a common statistical segment length b. The polymers are represented as continuous space curves, $\mathbf{R}_j^i(s)$, where i denotes the polymer species (A, B, or AB), j the different polymers of a component, and s represents the chain length variable measured along the chain backbone such that $0 \le s \le \nu_j$ with $\nu_{AB} = 1$ and $\nu_A = \nu_B = \alpha$. Conformations of noninteracting polymers are given a Gaussian statistical weight, $\exp(-H_0)$, with a harmonic stretching energy given by (units of $k_B T$)

$$H_0[\mathbf{R}] = \frac{3}{2Nb^2}\sum_i \sum_{j=1}^{n_j} \int_0^{\nu_j} \mathrm{d}s \left|\frac{\mathrm{d}\mathbf{R}_j^i(s)}{ds}\right|^2 \tag{2}$$

where $b_A = b_B = b_{AB} \equiv b$ is the statistical segment length. Interactions between A and B segments are modeled as local contact interactions by a pseudopotential with a Flory−Huggins quadratic form in the microscopic volume fractions,

$$H_I[\mathbf{R}] = \chi\rho_0 \int \mathrm{d}\mathbf{r}\, \hat{\phi}_A(\mathbf{r})\hat{\phi}_B(\mathbf{r}) \tag{3}$$

which with the substitutions $\hat{m} = \hat{\phi}_B - \hat{\phi}_A$, $\hat{\phi} = \hat{\phi}_A + \hat{\phi}_B$ transforms into

$$H_I[\mathbf{R}] = \frac{\chi r_0}{4}\int \mathrm{d}\mathbf{r}\, (\hat{\phi}^2 - \hat{m}^2) \tag{4}$$

χ denotes the Flory−Huggins parameter, and the microscopic density operators $\hat{\phi}_A$ and $\hat{\phi}_B$ are defined by

$$\hat{\phi}_A(\mathbf{r}) = \frac{N}{\rho_0}\sum_{j=1}^{n_{AB}} \int_0^f \mathrm{d}s\, \delta(\mathbf{r} - \mathbf{R}_j^{AB}(s)) + \frac{N}{\rho_0}\sum_{j=1}^{n_A} \int_0^\alpha \mathrm{d}s\, \delta(\mathbf{r} - \mathbf{R}_j^{A}(s)) \tag{5}$$

$$\hat{\phi}_B(\mathbf{r}) = \frac{N}{\rho_0}\sum_{j=1}^{n_{AB}} \int_f^1 \mathrm{d}s\, \delta(\mathbf{r} - \mathbf{R}_j^{AB}(s)) + \frac{N}{\rho_0}\sum_{j=1}^{n_B} \int_0^\alpha \mathrm{d}s\, \delta(\mathbf{r} - \mathbf{R}_j^{B}(s)) \tag{6}$$

Furthermore, the incompressibility constraint is implemented by the insertion of a Dirac delta functional,[46] and we obtain the canonical partition function of the blend, $\mathcal{Z}_C$

$$\mathcal{Z}_C \propto \int \prod_i \prod_j D\mathbf{R}_j^i(s)\, \delta(\hat{\phi} - 1) \exp(-H_0 - H_I) \tag{7}$$

where the $\int D\mathbf{R}$ denote functional integrations over chain conformations. Representing the delta functional in exponential form and employing a Hubbard−Stratonovich transformation on the $\hat{m}^2$ term in (4), we obtain

$$\mathcal{Z}_C \propto \int \prod_\infty DW_- \prod_{i\infty} DW_+ \exp[-H_C(W_-, W_+)] \tag{8}$$

with

$$H_C(W_-, W_+) = C\left[\frac{1}{\chi N}\int \mathrm{d}\mathbf{r} W_-^2 - \int \mathrm{d}\mathbf{r} W_+ - V(1 - \phi_H)\ln Q_{AB} - \frac{V\phi_H}{2\alpha}(\ln Q_A + \ln Q_B)\right] \tag{9}$$

$$C = \frac{\rho_0}{N} R^d \tag{10}$$

Here and throughout this article, all lengths are ex-

pressed in units of the unperturbed radius of gyration, $R_{g0} = b(N/(2d))^{1/2}$, where d is the space dimension. The parameter C in the above equations, which occurs as a global prefactor to H_C, acts as a Ginzburg parameter such that in the limit $C \rightarrow \infty$ the partition function (8) is dominated by its saddle point and the mean-field solution becomes exact. In (9), $i \equiv \sqrt{-1}$, and Q_A, Q_B, and Q_{AB} denote respectively the single-chain partition functions for the A, B, and AB chains, in the potential fields $W_-(\mathbf{r})$ and $W_+(\mathbf{r})$. Note that W_- is conjugate to the difference in A and B densities, $\hat{m}$, and W_+ to the total density, $\hat{\phi}$. Moreover, W_- is real, whereas W_+ is imaginary, thereby rendering H_C complex.

The single-chain partition functions can be expressed in terms of the Feynman−Kac formulas[21] as

$$Q_i = \int \mathrm{d}\mathbf{r}\; q_i(\mathbf{r}, \nu_i) \tag{11}$$

where the propagators q_i satisfy the diffusion equations

$$\frac{\partial}{\partial s} q_i(\mathbf{r}, s) = \Delta q_i(\mathbf{r}, s) - q_i U_i; \quad q_i(\mathbf{r}, 0) = 1 \tag{12}$$

$$U_A = W_+ - W_-, \quad 0 \le s \le \alpha$$
$$U_B = W_+ + W_-, \quad 0 \le s \le \alpha \tag{13}$$
$$U_{AB} = \begin{cases} U_A, & 0 \le s \le f \\ U_B, & f \le s \le 1 \end{cases}$$

An analogous diffusion equation applies to the conjugate propagators, $q^\dagger_i$, which propagate from the opposite end of a polymer. Because of their symmetry, the propagators of the homopolymers are their own conjugates. Hence, we can calculate density operators, $\bar{\phi}_A$ and $\bar{\phi}_B$, from

$$\bar{\phi}_A(\mathbf{r}) = \frac{V(1-\phi_H)}{Q_{AB}} \int_0^f \mathrm{d}s\; q_{AB}(\mathbf{r}, s)\, q^\dagger{}_{AB}(\mathbf{r}, 1-s) + \frac{V\phi_H}{2\alpha Q_A} \int_0^\alpha \mathrm{d}s\; q_A(\mathbf{r}, s)\, q_A(\mathbf{r}, \alpha - s) \tag{14}$$

$$\bar{\phi}_B(\mathbf{r}) = \frac{V(1-\phi_H)}{Q_{AB}} \int_f^1 \mathrm{d}s\; q_{AB}(\mathbf{r}, s)\, q^\dagger{}_{AB}(\mathbf{r}, 1-s) + \frac{V\phi_H}{2\alpha Q_B} \int_0^\alpha \mathrm{d}s\; q_B(\mathbf{r}, s)\, q_B(\mathbf{r}, \alpha - s) \tag{15}$$

These d shown on these snapshots are not to be confused with real density operators depend on W_- and W_+ and are in general complex. However, their ensemble averages yield real densities which correspond to the experimentally measurable quantities: $\phi_{A,B} = \langle\hat{\phi}_{A,B}\rangle (= \langle\hat{\phi}_{A,B}\rangle)$.

The above derivation assumed a canonical ensemble for the blend, wherein the average compositions of the different compositions are fixed. For future reference, we also list a similar set of formulas obtained in the grand-canonical ensemble:

$$H_{GC}(W_-, W_+) = C\left[\frac{1}{\chi N}\int \mathrm{d}r\; W_-{}^2 - \int \mathrm{d}\mathbf{r}\; W_+ - Q_{AB} - zQ_A - zQ_B\right] \tag{16}$$

where $z = \exp((\Delta\mu/k_BT)$, and $\Delta\mu \equiv \mu_A - \mu_{AB} = \mu_B - \mu_{AB}$ is the difference in the chemical potentials of homopolymers and copolymers. The density operators are given as

$$\bar{\phi}_A(\mathbf{r}) := \int_0^f \mathrm{d}s\; q_{AB}(\mathbf{r}, s) q^\dagger{}_{AB}(\mathbf{r}, 1-s) + z\int_0^\alpha \mathrm{d}s\; q_A(\mathbf{r}, s) q_A(\mathbf{r}, \alpha - s) \tag{17}$$

$$\bar{\phi}_B(\mathbf{r}) := \int_f^1 \mathrm{d}s\; q_{AB}(\mathbf{r}, s) q^\dagger{}_{AB}(\mathbf{r}, 1-s) + z\int_0^\alpha \mathrm{d}s\; q_B(\mathbf{r}, s) q_B(\mathbf{r}, \alpha - s) \tag{18}$$

III. Field-theoretic Simulations

A. General Considerations. Field-theoretic models like the one introduced above have been used in many earlier researches, and the resulting functional integrals of the partition function have been analyzed using various approximate methods. In self-consistent mean-field theory (SCFT),[10,25,47] the integrand of (8) is approximated by saddle points ($W_+{}^*$, $W_-{}^*$) such that

$$\frac{\delta H}{\delta W_+}|_{W_+{}^*, W_-{}^*} = 0, \frac{\delta H}{\delta W_-}|_{W_+{}^*, W_-{}^*} = 0 \tag{19}$$

A homogeneous saddle point then corresponds to the disordered phase, whereas every ordered phase has a unique inhomogeneous saddle point. By examining (8), it is further apparent that C plays the role of a Ginzburg parameter in the sense that the mean-field approximation, i.e., $Z \simeq \exp(-H[W_{+*}, W_-{}^*])$, becomes exact in the formal limit of $C \rightarrow \infty$, corresponding to $N \rightarrow \infty$ for $d > 2$. Implementations of SCFT[10] can thus be viewed as numerical strategies for computing the various saddle points. However, thermal fluctuation effects in the vicinity of phase boundaries invalidate the mean-field results in these regions, and strategies for evaluating (8) must be found. Analytical methods are quite limited, especially for systems dominated by inhomogeneous saddle points, and often involve weak segregation expansions.[34] In contrast, earlier publications of two of us[43−45] have detailed a new approach termed *field-theoretic simulations*, which is a methodology for numerically sampling functional integrals in field-theoretic models of polymer solutions and melts. The underlying idea is to numerically sample Z (independently of the type of ensemble employed) by generating a Markov chain of W_-, W_+ states with a stationary distribution proportional to $\exp(-H[W_-, W_+])$. Averages of physical quantities $\bar{f}[W_-, W_+]$ can then be approximated by "time" averages using the states of the Markov chain,

$$\langle\bar{f}[W_-, W_+]\rangle \approx 1/M\sum_{j=1}^{M} \bar{f}[W_{-,j}, W_{+,j}] \tag{20}$$

where j labels the states of the Markov chain. True equality of ensemble and time averages is established as usual for ergodic systems in the limit $M \rightarrow \infty$. Such a numerical method is nonperturbative in nature, allowing for a more complete account of fluctuation effects.

In this article, we undertake field-theoretic simulations to address the effect of fluctuations upon the mean-field phase diagram. Note that to numerically generate the Markov chain of W_-, W_+ states, one needs to account for the fact that $H[W_-, W_+]$ ((9) and (16)) in general possesses both real and imaginary parts, implying a nonpositive-definite statistical weight $\exp(-H)$. In our previous researches, we implemented a general "complex Langevin dynamics" technique that had been proposed earlier to deal with such nonpositive-definite

statistical weights.[48,49] In view of the fact that this method has been discussed in detail in our previous publications, we restrict our discussion to a brief outline of the technique which is presented in the Appendix. It is to be noted that outstanding issues still remain as regards the theoretical foundations of this technique.[48] While in our earlier studies we encountered no problems with the convergence or the uniqueness of the solutions, in the present study this method did encounter numerical difficulties, especially in the regions close to the Lifshitz point. These difficulties are associated with strong fluctuations and complex phase oscillations and will be described more fully in a subsequent section.

In an effort to probe and overcome the difficulties encountered in preliminary complex Langevin simulations of the present ternary blend and quantify the effect of fluctuations on the phase diagram of this system, we present an alternative, albeit equally rigorous technique for implementing field-theoretic simulations, which we refer to as the *field-theoretic Monte Carlo method*. In the discussion of our results, we compare explicitly the results obtained by the latter method with that obtained through the complex Langevin method and find good agreement in the range of their validities. It is pertinent to also note that there also exist real Langevin methods in the literature that focus specifically on the W_- fluctuations.[50]

B. The Field-Theoretic Monte Carlo Method. Our approach to sampling (8) is based on the Monte Carlo method. We recall that W_- is real and W_+ imaginary, and that the fluctuations in W_+ are conjugate to the total density. Although the incompressibility constraint implemented in our model effectively only constrains $\phi \equiv \phi_A + \phi_B = \langle \hat{\phi}_A + \hat{\phi}_B \rangle$, one might guess that the effect of the W_+ fluctuations that impose this constraint is rather small compared to the composition fluctuations governed by W_-. Therefore, we shall tackle W_- and W_+ in two distinct steps, after which we will be able to argue that the effect of the W_- fluctuations is indeed the dominant one.

To simulate the fluctuations in W_-, we pick a starting density configuration and use the SCFT mean-field equations[25] to calculate a seed W_- and W_+. Next, we proceed according to the following scheme:

(a) Make a global move in W_-; i.e., tentatively add a random number $\in[-1, +1]$ times a step width parameter to every $W_-(\mathbf{r})$, and denote by W_-^0 the old W_-.

(b) Calculate a self-consistent $\bar{W}_+$ that is a partial saddle point with the tentative new W_- fixed; to do this, we need to iteratively solve the equation

$$\bar{\phi}_A(\mathbf{r};[\bar{W}_+, W_-]) + \bar{\phi}_B(\mathbf{r};[\bar{W}_+, W_-]) = 1 \qquad (21)$$

for $\bar{W}_+(\mathbf{r})$. The initial guess for $\bar{W}_+$ in this iteration, $\bar{W}_+^0$, is taken to be the old $\bar{W}_+$ from the last Monte Carlo cycle. The iteration, which employs a two-step Anderson mixing scheme,[51] is terminated once $\Delta H \equiv H[W_-, \bar{W}_+] - H[W_-^0, \bar{W}_+^0]$ is determined to within 0.001, or a few parts in 10^4. Every step in this iteration requires the solution of the diffusion eq 12 on the entire simulation lattice, and this is where practically all the computing time is spent. The number of iterations to find $\bar{W}_+$ in most cases is roughly around 10.

(c) Accept or reject the move according to a standard Metropolis criterion. In other words, we always accept the move if the resulting difference in H, i.e., ΔH, is negative, and otherwise, we accept with a probability $\exp(-\Delta H)$.

(d) Go back to part a, unless the maximum number of Monte Carlo steps has been reached.

Next, we turn to discuss the sampling of W_+ fluctuations. As a result from SCFT, we know that the saddle point W_+^* of W_+ as well as the partial saddle point $\bar{W}_+[W_-]$ are purely real, despite the fact that the integration path of W_+ in (8) is along the imaginary axis. Neglecting surface terms and because we do not cross any singularities, we can therefore deform the integration path and represent W_+ as

$$W_+(\mathbf{r}) = \bar{W}_+[W_-](\mathbf{r}) + i\tilde{\omega}_+(\mathbf{r}) \qquad (22)$$

where $\bar{\omega}_+(\mathbf{r})$ is real. Furthermore, we split the argument of the integral in the partition function into a real part and a complex reweighting factor, leading to the following expression for the canonical ensemble:

$$Z_C \propto \int \mathcal{D}W_- \int \mathcal{D}\tilde{\omega}_+ \exp(-H_C^R) I_C \qquad (23)$$

$$H_C^R = C\left[\frac{1}{\chi N}\int d\mathbf{r}\, W_-^2 - \int d\mathbf{r}\, \bar{W}_+ - \sum_i \left(\frac{V_i}{\nu_i} \mathrm{Re}(\ln Q_i[W_-, \tilde{\omega}_+])\right)\right] \qquad (24)$$

$$I_C = \exp\left(C\left[i\int d\mathbf{r}\tilde{\omega}_+ + i\sum_i \frac{V_i}{\nu_i} \mathrm{Im}(\ln Q_i[W_-, \tilde{\omega}_+])\right]\right) \qquad (25)$$

where V_i is the volume occupied by species i. In the grand canonical ensemble the corresponding expression is

$$Z_{GC} \propto \int \mathcal{D}W_- \int \mathcal{D}\tilde{\omega}_+ \exp(-H_{GC}^R) I_{GC} \qquad (26)$$

$$H_{GC}^R = C\left[\frac{1}{\chi N}\int d\mathbf{r}\, W_-^2 - \int d\mathbf{r}\, \bar{W}_+ - \sum_i z_i \,\mathrm{Re}(Q_i[W_-, \tilde{\omega}_+])\right] \qquad (27)$$

$$I_{GC} = \exp(C[i\int d\mathbf{r}\, \tilde{\omega}_+ + i\sum_i z_i \,\mathrm{Im}(Q_i[W_-, \tilde{\omega}_+])]) \qquad (28)$$

where $z_{AB} = 1$ and $z_A = z_B = z$.

We can thus in principle simulate both W_- and W_+ fluctuations, e.g., by alternating a move in W_- with a number of moves in $\tilde{\omega}_+$ and replacing $\Delta H_{C,GC}$ with $\Delta H^R_{C,GC}$ in the Metropolis criterion. Each configuration then needs to be weighted with the factor $I_{C,GC}$ for the purpose of computing averages. We note that the propagators and the field term in the diffusion eq 12 are now complex, but the averages of all physical quantities will approach real values in equilibrium.

At this point, a remark concerning our numerical methods is due: the single most time-consuming part in doing our simulations is the solution of the diffusion equation, eq 12. Initially, we used either the Crank−Nicholson (CN) or DuFort−Frankel (DF) finite differencing schemes[52,53] to effectuate this task. As it turned out, however, a pseudo-spectral method that had been used successfully in the past to solve the mathematically very similar Schrödinger equation and that had recently been applied to SCFT[54,55] was far better suited for our needs. Typically, it allowed for an order of magnitude higher values of contour step ds than either CN or DF

to achieve the same accuracy. Implementing the scheme with highly optimized fast Fourier transform routines like the publicly available FFTW library,[56] the computing time per contour step is only roughly double that needed for DF and half that needed for CN on a single processor. We therefore regard it as the method of choice in the context of polymer field theory. For the larger system sizes to be discussed in the next section, a parallel version of the code was used.

C. Analysis of W_+ Fluctuations. Evidently, the W_+ fluctuations exert their influence on the simulation in two ways: (a) through the complex reweighting factor I_C or I_{GC} and (b) through the difference of ΔH^R from ΔH.

We consider first I_{GC} and to this end split the complex diffusion equation into two real equations for the real and imaginary parts of the propagator for polymers of type i, denoted q_i^R and q_i^I, respectively. Note the symmetry properties of this coupled set of equations with respect to a sign change in $\tilde{\omega}_+$: for $W_+ = \bar{W}_+ \pm i\tilde{\omega}_+$ we obtain

$$\frac{\partial}{\partial s}q_i^{\,R} = \Delta q_i^{\,R} - U_i q_i^{\,R} \pm \tilde{\omega}_+ q_i^{\,I}$$
$$\pm \frac{\partial}{\partial s}q_i^{\,I} = \pm \Delta q_i^{\,I} \mp U_i q_i^{\,I} - \tilde{\omega}_+ q_i^{\,R} \tag{29}$$

We see that q_i^R remains unchanged whereas q_i^I goes to $-q_i^I$. Thus, for the corresponding single-chain partition function $Q_i = Q_i^R + iQ_i^I$, Q_i^R is symmetric in $\tilde{\omega}_+$, and Q_i^I antisymmetric. Furthermore, the exponent of the reweighting factor I_{GC} is antisymmetric in $\tilde{\omega}_+$ (cf. (28)). Since in the partition function (26) we integrate over all possible configurations of $\tilde{\omega}_+$, the imaginary parts of I_{GC} cancel out for each antisymmetric pair, and consequently, we effectively only need to apply the real part of I_{GC}:

$$I_{GC}^{\,R} = \cos(C[\int \mathrm{d}\mathbf{r}\tilde{\omega}_+ + \sum_i z_i Q^I{}_i[W_-, \tilde{\omega}_+]]) \tag{30}$$

These symmetries reveal that in a functional expansion of Q_i in $\tilde{\omega}_+$ around the partial saddle point, $\bar{Q}_i[W_-]$, the even-order terms coincide with the expansion of Q_i^R, and the odd-order terms with that of Q_i^I. Moreover,

$$\frac{\delta Q_i}{\delta W_+} \equiv \frac{\delta Q_i^{\,I}}{\delta \tilde{\omega}_+} \tag{31}$$

and

$$\sum_i z_i \frac{\delta Q_i^{\,I}}{\delta \tilde{\omega}_+} = \sum_i z_i \frac{\delta Q_i}{\delta W_+} = -\langle \hat{\rho} \rangle = -1 \tag{32}$$

by virtue of the incompressibility constraint. Hence,

$$\sum_i z_i Q_i^{\,I} = -\int \mathrm{d}\mathbf{r}\tilde{\omega}_+ + \mathcal{O}(\tilde{\omega}_+{}^3) \tag{33}$$

and finally

$$I_{GC} = \cos(\mathcal{O}(\tilde{\omega}_+{}^3)) = 1 - \mathcal{O}(\tilde{\omega}_+{}^6) \tag{34}$$

$$Q_i^{\,R} = \bar{Q}_i[W_-] + \mathcal{O}(\tilde{\omega}_+{}^2) \tag{35}$$

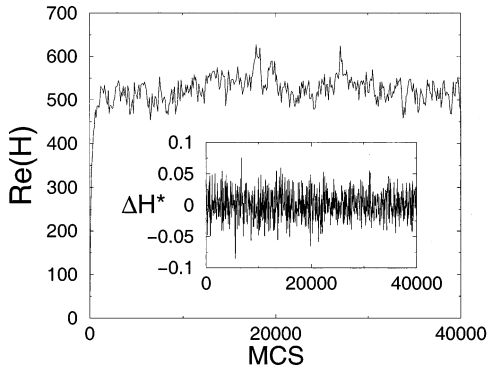

Figure 3. Re(H) in a simulation of W_- and W_+ vs number of Monte Carlo steps in W_- for $C = 50$, $\chi N = 12$, and $z = 2$ (grand canonical ensemble), started from a configuration equilibrated in W_-. Each W_- step alternates with 10 steps in $\tilde{\omega}_+$. Inset shows ΔH^* (difference of ΔH and a reference value at $\tilde{\omega}_+$ fluctuations switched off) in the same simulation.

On the basis of these analytical results, we should expect I_{GC} to deviate only very slightly from unity so that it can be neglected in most practical cases. Hence, the impact of the W_+ fluctuations would materialize solely as a (real) $\mathcal{O}(\tilde{\omega}_+{}^2)$ contribution to H_{GC}. The above derivation of (34) and (35) was for the grand canonical ensemble but holds true if one is to derive analogous relations in the canonical ensemble, as well, because the leading term of ln Q_i is linear in $\tilde{\omega}_+$, as in the grand canonical ensemble. It should however be noted that in the canonical ensemble, the gauge invariance of the theory to a constant shift of the $\tilde{\omega}_+$ field allows the introduction of a spurious phase factor $e^{i\psi}$ that preserves H_C (and hence $|Q_i|$ and H^R). This ψ field will freely move in canonical simulations unless constrained, e.g., by demanding that $\int \mathrm{d}\mathbf{r}\tilde{\omega}_+(\mathbf{r}) = 0$. In contrast, in the grand canonical ensemble, Q^R and hence H^R are to lowest approximation quadratic functions around $\tilde{\omega}_+ = 0$. As a result, the shape of the $H^R(W_+)$ energy landscape is much steeper in the grand canonical ensemble than in the canonical, and no constraint is needed.

While the above considerations can only give us an indication of the insignificance of the W_+ fluctuations, we have also done test simulations to get more conclusive estimates. We therefore choose the grand canonical ensemble for testing our simulation technique of W_+ fluctuations. Before starting a run at $z = 2$, $\chi N = 12$, $\alpha = 0.2$, and $C = 50$, we fully equilibrated a simulation of W_- fluctuations only with the same parameters, which started from a disordered configuration and ran a million Monte Carlo steps. This set of parameters is very close to the (fluctuation-corrected) order−disorder transition in the phase diagram, on the disordered side. The average homopolymer fraction, ϕ_H, is 0.65. On a 32 × 32 lattice with periodic boundary conditions, we used $\mathrm{d}x = 0.78125$. We then took this equilibrated configuration and switched on the W_+ fluctuations, again making 10 (global) moves in W_+ after each move in W_- so as to roughly spend equal amounts of computing time for the two types of moves. Note in Figure 3 how H_{GC} quickly increases and then plateaus off, indicating that the W_+ fluctuations have become saturated.

For the same run, we recorded the quantity $\Delta H^* = \Delta H^R - \Delta H$ (cf. Equations 24 and 27), which is displayed in the inset of Figure 3. One can interpret $\sqrt{\langle(\Delta H^*)^2\rangle}$ as a measure for the deviation of the simulation from a reference case in which only W_- fluctuations are simulated. This simulation was done with a chain-contour

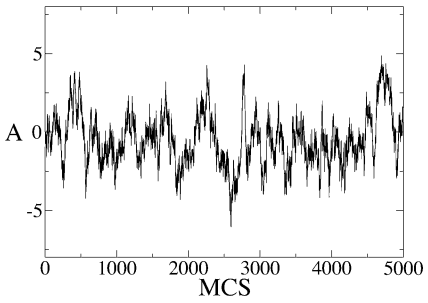

Figure 4. Argument, *A*, of the cosine in the reweighting factor in the same simulation as in Figure 3.

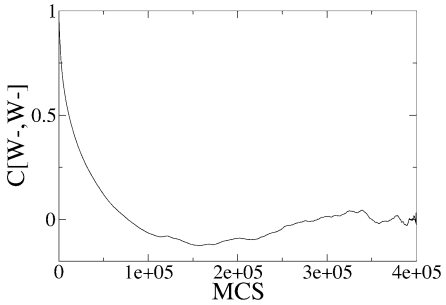

Figure 5. Autocorrelation function of W_- in the same simulation as in Figure 3.

discretization of d$s = 0.01$, which allows for the calculation of ΔH to within 0.01. Typically, in simulations involving the W_- field alone, we used d$s = 0.05$ in order to save computing time. The discretization error of ΔH in this case is increased to $\lesssim 0.08$. Considering that typical values of ΔH are on the order of ± 3, this appears like a very moderate numerical error. At the same time, we realize that the effect of the fluctuations in W_+ expressed through ΔH^* is well below our standard numerical accuracy: $\sqrt{\langle(\Delta H^*)^2\rangle} \approx 0.022$. Furthermore, the average of ΔH^* very closely approximates zero, so there is no drift of ΔH as a result. We therefore conclude that contributions of the W_+ fluctuations to H^R cannot be distinguished as such from numerical inaccuracies.

Next, we examine the reweighting factor, I_{GC}, in the particular simulation discussed above. Numerically, we must evaluate:

$$I_{GC}{}^{R} = \cos(C[\int \mathrm{d}\mathbf{r}\tilde{\omega}_+ + \sum_i z_i Q_i^{I}]) \equiv \cos(A) \quad (36)$$

The two terms in the argument, *A*, of the cosine in (36) have opposite signs and largely cancel out each other, as was demonstrated theoretically above. However, in practice, the numerical application of I_{GC} to the simulation is impeded greatly by the fact that the two contributions to *A* are extensive, so the fluctuations in *A* are amplified. I_{GC} is a nonpositive-definite weighting factor, echoing the well-known "sign problem" encountered in fermionic field theories in elementary particle physics.[57] Figure 4 displays part of a time series of *A* in our above test run. It performs fast oscillations around a very small absolute mean value which within numerical accuracy closely approximates zero when averaged over the entire run, although it is expected from theory to be finite. This is the essence of our sign problem: the statistical deviation from the mean completely dominates *A*. At this point, we seem to have arrived at a dead end, having to concede that we cannot numerically implement the reweighting factor. However, we still may get a sense of the impact of the $\tilde{\omega}_+$ fluctuations from examining pairwise correlation functions of $\tilde{\omega}_+$, W_-, and I_{GC}. The correlation function is defined as

$$C[A, B; t] = \frac{\langle A(t')B(t'+t)\rangle - \langle A\rangle\langle B\rangle}{\sigma_A{}^2\sigma_B{}^2} \quad (37)$$

where σ denotes standard deviation, and t and t' are numbers of moves in W_-. If *A* or *B* is a field, we average over all lattice points **r**. Figure 5 shows $C[W_-, W_-]$, and in Figure 6, $C[I, I]$,$C[\tilde{\omega}_+, \tilde{\omega}_+]$, $C[I, W_-]$, and $C[\tilde{\omega}_+, W_-]$ are displayed. On comparing the various correlation times, an important qualitative difference is observed:

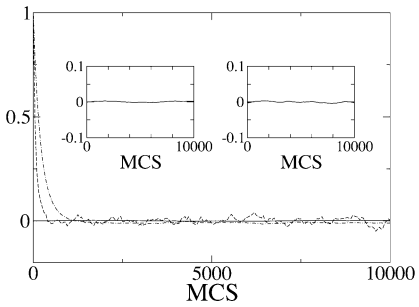

Figure 6. Correlation functions $C[I,I]$ (dashed), $C[\tilde{\omega}_+,\tilde{\omega}_+]$ (dashed−dotted), $C[I,W_-]$ (left inset), and $C[\tilde{\omega}_+,W_-]$ (right inset) in the same simulation as in Figure 3. Note the different scale from Figure 5.

while the autocorrelation time of W_- is on the order of 10^5 Monte Carlo steps in W_- (subsequently denoted MCS), those of $\tilde{\omega}_+$ and *I* are only on the order of a few hundred MCS, i.e., several orders of magnitude smaller.[58] Furthermore, the correlation functions of W_- with both $\tilde{\omega}_+$ and *I* are virtually flat lines, indicating the absence of any cross-correlations. The same is obtained for $C[\tilde{\omega}_+, W_-{}^2]$.

With this result in mind, consider again the partition function (26). We demonstrated before that we may essentially replace$H^R[W_-, \tilde{\omega}_+]$ with $H[W_-]$ and so rewrite Z_{GC} as

$$Z_{GC} \propto \int \mathscr{D}W_- \mathrm{e}^{-H_{GC}} \int \mathscr{D}\tilde{\omega}_+ I_{GC}[W_-, \tilde{\omega}_+] \quad (38)$$

Since, as we have seen, *I* and W_- are virtually uncorrelated, we argue that the results of the simulation of W_- cannot possibly be altered by the reweighting factor in a significant way.

In sum, the results of these test simulations indicate that the W_+ fluctuations do not influence the structure of the polymer blends substantially. Therefore, the Monte Carlo simulations presented in the next section were restricted to W_- fields only.

IV. Results and Discussion

We have studied the two-dimensional ternary A + B + AB system at dimensionless number density $C = 50$. In evaluating these simulations, we must establish two phase boundaries: first, the fluctuation-shifted order−disorder transition, and second, the onset of the phase-separated region. For the former, two parameters have been used which we shall define in the following.

The Direction Persistence Parameter. To define and determine this parameter, a given distribution $W_-(\mathbf{r})$ is translated via (15) into a "density" pattern $\bar{\phi}_A(\mathbf{r})$. All simulations performed with the field-theoretic Monte Carlo method that are presented in this section

took only W_- fluctuations into account. Hence, $\bar{\phi}_A(\mathbf{r})$ is real. Lattice points are denoted black if $\bar{\phi}_A(\mathbf{r})) < 0.5$, and white if $\bar{\phi}_A(\mathbf{r})) \geq 0.5$. We further define $\langle \max(l_a) \rangle$ as the maximal length of either black or white sections along a one-dimensional cross section of the image in direction **a**, averaged over all offsets along the X axis (or equivalently the Y axis). The direction persistence parameter, Λ, is defined for a two-dimensional black-and-white image as

$$\Lambda := <\frac{\langle \max(l_{||}) \rangle}{\langle \max(l_{\perp}) \rangle}|_{\text{all directions}} - 1 \tag{39}$$

where $l_{||}$ denotes the direction being averaged over, and $l_\perp$ the direction perpendicular to a given $l_{||}$. Λ is 0 in a disordered configuration and positive definite in a lamellar configuration, and thus constitutes a measure for the "lamellarness" of a configuration. Furthermore, it is dimensionless and does not directly depend on the lattice size. Λ measures lamellarness from a local perspective.

Anisotropy Parameters. As a complementary measure of anisotropy, we define the parameters $\bar{F}_2$ and $\bar{F}_4$, which measure the anisotropy of the Fourier transform, $F(\boldsymbol{q})$, of a $\bar{\phi}_A(\mathbf{r})$ image to look at periodicity from a more macroscopic point of view:

$$F_n(q) := \frac{1}{2\pi} \left| \int_0^{4\pi} \mathrm{d}\phi |F(\mathbf{q})|^2 e^{\mathrm{i}n\phi} \right| \tag{40}$$

By definition, F_2 and F_4 are identically zero in a disordered (isotropic) configuration and are positive otherwise. A more convenient way to analyze $F_n(q)$ is to calculate a normalized ratio of the integral and the standard deviation of $F_n(q)$, which yields a single dimensionless number:

$$\bar{F}_n := \frac{\int \mathrm{d}q\, F_n(q)}{\sigma(q)|_{F_n}} \tag{41}$$

$$\sigma(q)|_{F_n} \equiv \left[\frac{\int \mathrm{d}q\, q^2 F_n(q)}{\int \mathrm{d}q\, F_n(q)} - \left(\frac{\int \mathrm{d}q\, q F_n(q)}{\int \mathrm{d}q\, F_n(q)} \right)^2 \right]^{1/2} \tag{42}$$

$\bar{F}_n$, like $F_n(q)$, is 0 for disordered and nonzero for lamellar configurations. Note that $F(\mathbf{q})$ is not the structure factor of the melt but simply the Fourier transform of $\bar{\phi}_A$. In fully equilibrated simulations, the structure factor can be calculated from averaged expressions containing the fields W_- and W_+.[44]

A. Monte Carlo Simulations. We shall first discuss the results of the Monte Carlo simulations.

The shift of the order−disorder transition was examined in the canonical ensemble on a 32×32 lattice with $\mathrm{d}x = 0.625$ for $\phi_H = 0$ and 0.2, and $\mathrm{d}x = 0.78125$ for $\phi_H = 0.4$, 0.6, and 0.7. These $\mathrm{d}x$ values were chosen such that a single lamella was several pixels wide, which is a precondition for the evaluation of the Λ parameter to work properly. For simplicity, we shall subsequently denote runs that started from a disordered configuration "D-started" and those that started out of a lamellar configuration, "L-started." In the latter, the lamellar periodicities of the starting configurations reflect the mean-field values at the given parameters. Moreover, in L-started runs, $\mathrm{d}x$ was chosen to allow for an integer number of lamellae to fit in the simulation box.

Figure 7. Snapshots at $C = 50$, $\phi_H = 0$, and $\chi N = 11.1$, 11.2, 11.3, 11.4, and 11.5. White points: $0 < \bar{\phi}_A < 0.49$. Gray points: $0.49 \leq \bar{\phi}_A < 0.51$. Black points: $0.51 \leq \bar{\phi}_A \leq 1$. All runs were started from disordered configurations.

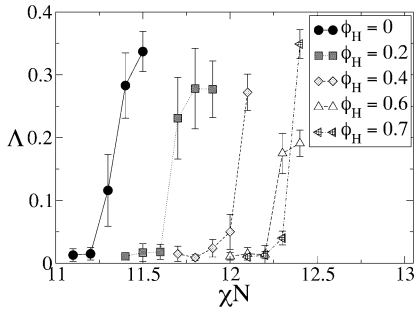

Figure 8. Direction persistence as measured by the Λ parameter vs χN for different homopolymer volume fractions ϕ_H at the order−disorder transition in simulations on 32×32 lattices. For $\phi_H = 0$ and 0.2, the discretization $\mathrm{d}x = 0.625$ was used; otherwise, $\mathrm{d}x = 0.78125$.

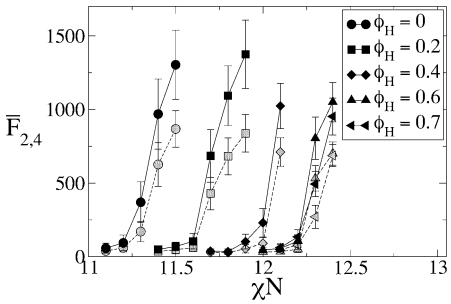

Figure 9. $\bar{F}_2$ (solid) and $\bar{F}_4$ (dahsed) vs χN for different homopolymer volume fractions ϕ_H at the order−disorder transition in the same simulations as in Figure 8.

In the case of copolymers only ($\phi_H = 0$), D-started runs at various χN yield the snapshots of Figure 7, which were taken after approximately 1 million Monte Carlo steps and after the simulations were equilibrated. It is clearly visible from the images that above a certain threshold χN, a lamellar phase begins to form spontaneously. We did not observe any hysteresis effects. We should stress that the patterns $\bar{\phi}_A(\mathbf{r})$ shown on these snapshots are not to be confused with real density patterns—they are merely visualizations of the field distributions $W_-(\mathbf{r})$.

To quantify the transition, we have plotted Λ in Figure 8 and $\bar{F}_2/\bar{F}_4$ in Figure 9. These plots also include curves for the other runs described above, i.e., homopolymer volume fractions ϕ_H up to 0.7. In all cases, a jump is displayed in both the Λ and $\bar{F}_2/\bar{F}_4$ parameters at the fluctuation-corrected critical χN. For $\phi_H = 0$, we find the transition to be shifted from the mean-field value of 10.495 to 11.3(1), which is in good agreement with a result obtained earlier by two of us with the complex Langevin method.[43] It is also further evidence that the W_+ fluctuations contribute only a minor correction to the partition function.

For homopolymer concentrations ϕ_H above 0.7 the configurations did not spontaneously assemble into a lamellar phase for any χN in D-started simulations on 32×32 lattices. The configurations can at best be described as very defective lamellae. However, in L-started runs the configurations only broke up at very

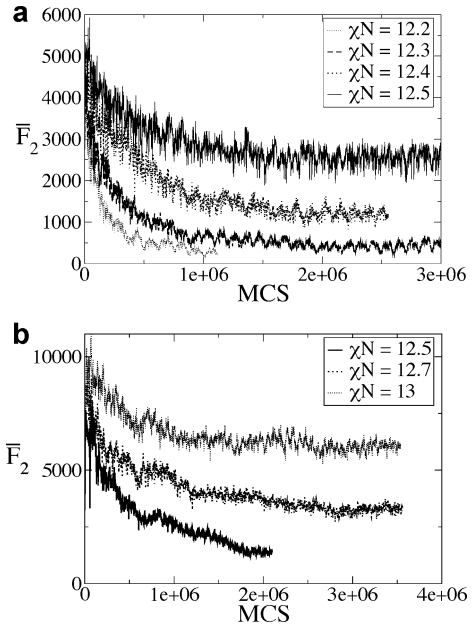

Figure 10. $\bar{F}_2$ at homopolymer volume fraction $\phi_H = 0.7$ (a) and $\phi_H = 0.8$ (b) for different χN in simulations on a 48 × 48 lattice that started from lamellar configurations.

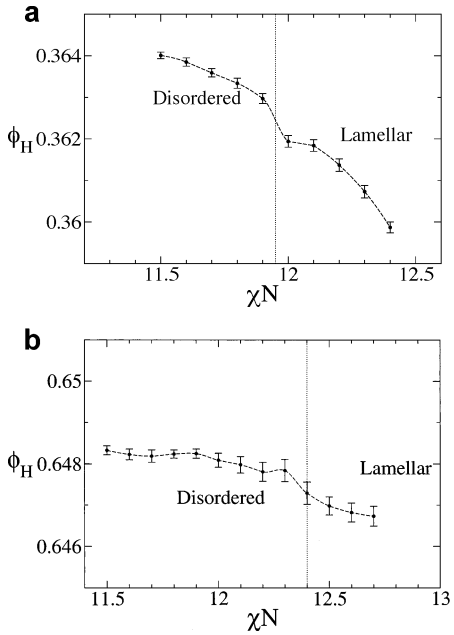

Figure 11. Homopolymer concentration, Φ_H, vs χN at $z = 1$ (a) and $z = 2$ (b) across the order−disorder transition. The dotted line indicates the χN coordiante of the ODT ±0.1.

low χN values. For example, at $\phi_H = 0.85$, D-started runs were done for $\chi N \leq 13$, all of which stayed disordered, yet in L-started runs the lamellae only broke up for $\chi N < 12.1$. This obvious discrepancy can be made plausible by two arguments: First, in the D-started runs, as we approach higher χN values (which correspond to lower temperatures), we observe a freezing effect, i.e., the simulations get trapped in configurations with a certain degree of *local* periodicity yet the systems cannot move through configuration space efficiently enough to achieve quasi-long-range order. Second, in the L-started runs, to keep d*x* reasonably low (i.e., $\lesssim$0.8), we can only put a small number of lamellae in the box. In the case of $\phi_H = 0.85$, that number is 3. But this in combination with the periodic boundary conditions imposed on the box in turn artificially stabilizes the lamellar phase, which is why we do not see a breaking up. Evidently, we must use bigger simulation boxes for $\phi_H \gtrsim 0.7$.

Because of the freezing effects at high χN described above, we restrict ourselves to L-started runs in examining the order−disorder transition on 48 × 48 lattices. Even so, we find that the simulations take an increasingly greater number of Monte Carlo steps to equilibrate the higher χN. For $\phi_H = 0.7$, a time series of $\bar{F}_2$ is displayed in Figure 10a. The plot indicates that the transition must be between $\chi N = 12.3$ and 12.5: we see a substantial jump in both parameters, caused by a breaking-up of the initial lamellar configuration. This is in good agreement with the result from the 32 × 32 lattice. The $\bar{F}_2$ graphs at the transition, especially for $\chi N = 12.3$, display a special feature: a periodic oscillatory motion once the run is equilibrated. The time scale of this oscillation can be explained as follows. Close to the transition, the lamellae do not easily dissolve completely. Instead, defects develop which may open and close periodically, often alternating the continuation of a given contour length between two defective lamellar branches. This oscillation is reflected in $\bar{F}_2$.

For $\phi_H = 0.8$, the corresponding time series is displayed in Figure 10 (b). At $\chi N = 12.5$, the system is clearly disordered, and the transition is inferred to occur below $\chi N = 13$. Another run for $\phi_H = 0.85$ indicates that that transition is at approximately $\chi N = 13$, although even after 3 million Monte Carlo steps the configurations retained a strong correlation to the seed configuration. We conclude that on one hand, using a bigger lattice has alleviated the artificial stabilizing effect of the periodic boundary conditions on the lamellae. On the other hand, however, we still encounter numerical freezing effects for $\chi N \gtrsim 13$ at $C = 50$, which prohibit the examination of this region of the phase diagram.

As concerns the order of the ODT, we did sweeps in the grand canonical ensemble across the ODT for relative homopolymer fugacities $z = 1$ and $z = 2$ (Figure 11). Both plots are consistent with a very weakly first-order transition. In either case, the coexistence region has a width of no more than approximately 0.001 in Φ_H.

The onset of the (macro) phase-separated two-phase region was examined in the grand canonical ensemble; a D-started run at parameters in the phase-separated region will eventually undergo a spontaneous symmetry breaking and end up in a configuration dominated by either A or B segments. Moreover, it is sufficient to do these runs on 32 × 32 lattices as no complex morphologies are investigated here. To quantify this behavior, we analyze the total difference of normalized A and B densities:

$$\Delta\phi := |V^{-1}\int \mathrm{d}\mathbf{r}\,(\bar{\phi}_A(\mathbf{r}) - \bar{\phi}_B(\mathbf{r}))| \qquad (43)$$

First, we looked at the demixing in a system consisting only of A and B homopolymers ($\phi_H = 1$). In this case, Figure 12 shows how the order parameter $\Delta\phi$ grows from zero above approximately 2.04/α, shifted up from the mean-field value of 2/α. For various χN, Figure 13 displays $\Delta\phi$ for relative homopolymer fugacities *z* (corresponding to $\phi_H < 1$ in the canonical ensemble) around the transition. When translated into ϕ_H values in the canonical ensemble, the numerical accuracy obtained in the present work did not allow for determining the order of the corrected disorder/two-phase transition.

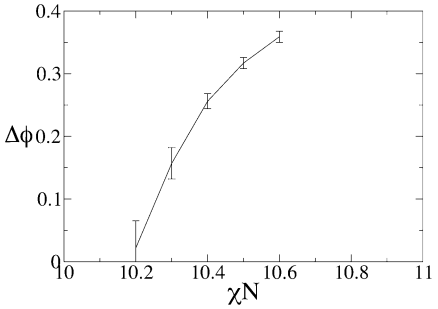

Figure 12. Difference of A and B monomer densities, $\Delta\phi$, vs χN in a binary system of A and B homopolymers in the grand canonical ensemble.

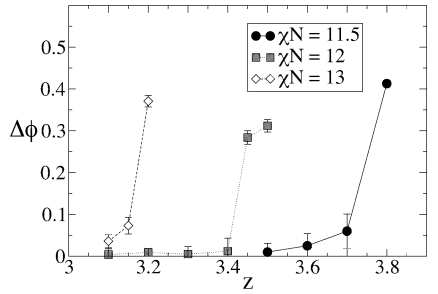

Figure 13. Difference in A and B monomer densities, $\Delta\phi$, vs relative homopolymer fugacity, z, in the grand canonical ensemble.

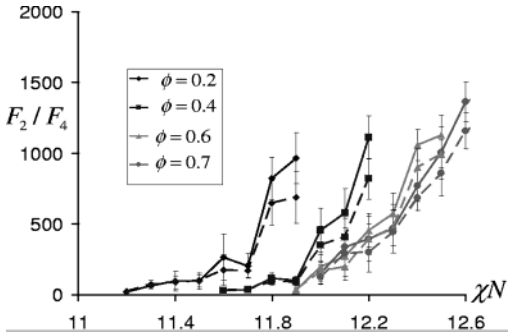

Figure 14. Anisotropy parameters obtained by complex Langevin simulations. The solid lines correspond to the $\bar{F}_2$ values while the dotted lines correspond to the $\bar{F}_4$ values.

B. Complex Langevin Simulations. The same system has also been examined by complex Langevin simulations for selected parameter values in the canonical ensemble. The simulations were initiated from L-started configurations (in the lamellar phase) to examine the shift in the ODT. The transition points were identified by examining the values of the anisotropy parameters $\bar{F}_2$ and $\bar{F}_4$. The behavior of these quantities (displayed in Figure 14) is quite similar to that observed in the field-theoretic Monte Carlo approach, and exhibits a steep increase near the onset of microphase separation. As an additional pictorial proof of such a transition, Figure 15 displays the averaged values of the *real* component of the fluctuating density fields across the transition.

As mentioned earlier in the text, complex Langevin simulations were hindered by numerical constraints arising from extensive phase fluctuations near the Lifshitz point, and required small time steps to maintain numerical stability. However, the use of such time steps led to freezing effects and rendered equilibration difficult. Consequently, we have displayed the results from CL simulations only for situations (i.e., ϕ_H values) for

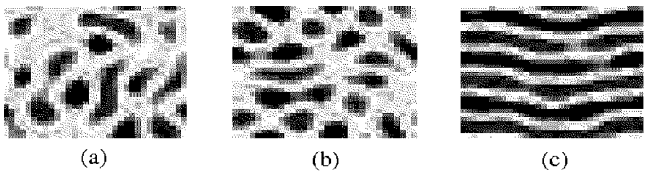

Figure 15. Averaged densities across the ODT, as obtained from complex Langevin simulation runs. The homopolymer fraction is fixed at $\Phi_H = 0.2$. The χN values are as follows: (a) $\chi N = 11.4$; (b) $\chi N = 11.7$; (c) $\chi N = 11.9$.

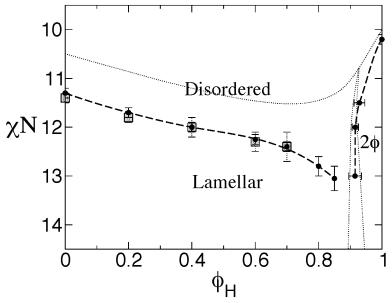

Figure 16. Fluctuation-corrected phase diagram at $C = 50$. The circles show the results from the Monte Carlo simulations and the squares those from the complex Langevin simulations. The dotted lines indicate the mean-field result of Figure 2.

which the fluctuation-corrected transition temperatures could be identified reliably. It is encouraging to note that the results obtained from the CL simulations, the basis of which is somewhat distinct from the field-theoretic Monte Carlo method presented in this article, do indicate very good agreement with the results of the latter approach. The implications of such results are 3-fold: (i) This serves to corroborate the results presented in earlier sections which were obtained using the Monte Carlo method. (ii) It also suggests that the fluctuation effects in the W_+ field, which were neglected in the Monte Carlo simulations (but which were included in the CL approach), have only a negligible influence upon the majority of the phase diagram. (iii) Furthermore, the coincidence of CL results with the Monte Carlo approach suggests that despite the tenuous foundations of complex Langevin approach, such a method does yield physically reliable results for a major portion of the phase diagram and thereby warrants further studies using such an approach.

C. The Fluctuation-Corrected Phase Diagram and the Formation of the Microemulsion. The results of our simulation investigations are put together in the fluctuation-corrected phase diagram for $C = 50$ (Figure 16) and lead to a slope of the resulting fluctuation-corrected order−disorder transition which is in good qualitative agreement with the experimental result of Hillmyer et al. for a PEE/PDMS/PEE−PDMS system of intermediate molecular weights.[19] In particular, the shape of the cusplike region of bicontinuous microemulsion identified therein is here reproduced computationally for the first time. It is important to note that to minimize computational expense our simulations were carried out in two dimensions, while the experiments are inherently three-dimensional. In general, one would expect the fluctuation effects to be stronger in 2-d than in 3-d, and indeed, the microemulsion "cusp" appears broader in Figure 16 than in the experimental phase diagrams. Nevertheless, we believe that a firm qualitative correspondence between simulation and experiment has been established.

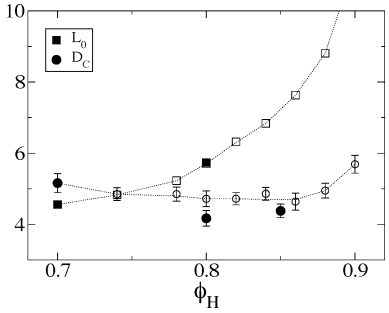

Figure 17. Curvature radius D_C (circles) and preferential length scale, L_0, as obtained from the maximum of $S_0(q)$ (squares) at $\chi N = 12.5$ in simulations on a 48 × 48 lattice. Filled and empty symbols correspond to disordered and lamellar initial conditions, respectively. Dashed lines are guies for the eye.

To understand better what happens at the onset of the microemulsion phase, we have calculated the mean curvature diameter, D_C, of the boundaries of A and B microdomains:

$$D_C = 2\left[\frac{1}{L_c}\int \mathrm{d}s \left|\frac{\mathrm{d}\mathbf{t}}{\mathrm{d}s}\right|^2\right]^{-1/2} \tag{44}$$

where L_c is the sum of all contour lengths of the microdomain boundaries, and **t** is the tangent vector at a given coordinate s along the contour. Details of the calculation of this object will be presented elsewhere.[59] Furthermore, we examine the maximum, q_{max}, of $\bar{F}_0(q)$, which indicates the preferential Fourier wavenumber of a configuration multiplied by 2π. In turn, $L/q_{max} =: L_0$ indicates the preferential length scale of a configuration. Figure 17 compares D_C and L_0 for various homopolymer concentrations ϕ_H at $\chi N = 12.5$, for both L-started and D-started runs. Whereas for lower ϕ_H, D_C is larger than L_0, the two lengths cross each other as ϕ_H is increased. Thus, we have identified the mechanism by which fluctuations generate the microemulsion phase: it forms when the width of the lamellae grows larger than the curvature radius of the fluctuating boundaries, causing the lamellae to break up. This type of "Lindemann criterion" for production of a bicontinuous microemulsion by melting of a lamellar phase has discussed elsewhere in the context of oil/water/surfactant phases.[60]

V. Summary and Conclusions

In the present paper, we have introduced a new way of evaluating the full partition function of a system of polymeric blends subject to thermal fluctuations. The complex Langevin approach which was employed in our earlier researches, accounts for both the W_- and W_+ fluctuations and is able to predict the shift in the order−disorder transition at low ϕ_H and in the two-phase region. For $0.7 \lesssim \phi_H \lesssim 0.9$, it runs into numerical difficulties. We believe that the large system sizes necessitated in such regions as well as the concomitant strong fluctuation effects arising near the Lifshitz points restricts the applicability of the complex Langevin method in such regimes. As an alternative, we have proposed a field-theoretic Monte Carlo approach, which was shown to be applicable to greater regions of the phase diagram. Small lattices (32 × 32) sufficed up to $\phi_H = 0.7$, above which bigger (48 × 48) lattices had to be used. In the region where both methods work, they are in good agreement, indicating that the W_+ fluctuations neglected in the latter simulations contribute only a minor correction. Further evidence for this circumstance was found in empirical test runs. Such observations also suggest that one could have potentially employed a real Langevin scheme where the W_+ fluctuations are neglected.[50] Regretfully, however, a full analysis of the W_+ fluctuations was rendered difficult by the occurrence of a nonpositive-definite weighting factor (the sign problem). A fluctuation-corrected phase diagram was presented for $C = 50$, which corresponds well in qualitative terms to the PEE/PDMS/PEE−PDMS system of intermediate polymerization indices examined in a series of recent experiments,[16−19] providing further corroboration of the existence of a region of bicontinuous microemulsion between the lamellar and phase-separated regions. The mechanism responsible for the formation of this phase was shown to be intimately related to matching length scales of the curvature of microdomain boundaries and of the lamellar periodicity. In an upcoming article, we will examine properties of the disordered phase.[59]

Acknowledgment. We have benefited from fruitful discussions with M. Schick, R. Netz, M. Matsen, and S. Sides. This work was supported by the Deutsche Forschungsgemeinschaft (Germany). VG and GHF were partially supported by the National Science Foundation under Awards DMR-02-04199 and DMR-98-70785, and the donors of the Petroleum Research Fund, administered by the American Chemical Society. The Monte Carlo simulations were carried out on the CRAY T3E of the NIC institute in Jülich, Germany.

Appendix: Complex Langevin Method

In this appendix, we provide a brief outline of the complex Langevin method. Readers interested in more details are referred to ref 44. The complex Langevin technique involves generating W_- and W_+ states *in the entire complex plane* (despite the fact that the integrations in eq 8 are restricted to the real axis in W_- and the imaginary axis in W_+) by means of *complex Langevin* equations. Specifically, the equations used to generate the real and imaginary parts of the W_- and W_+ fields, W_-^R, W_-^I, W_+^R, and W_+^I, are of the form

$$\frac{\partial[W_-^R(\mathbf{r}, t)+iW_-^I(\mathbf{r}, t)]}{\partial t} = -\frac{\delta H[W_-, W_+]}{\delta W_-(\mathbf{r}, t)} + \theta(\mathbf{r}, t) \tag{45}$$

$$\frac{\partial[W_+^I(\mathbf{r}, t) - iW_+^R(\mathbf{r}, t)]}{\partial t} = -i\frac{\delta H[W_-, W_+]}{\delta W_+(\mathbf{r}, t)} + \theta(\mathbf{r}, t) \tag{46}$$

where $\theta(\mathbf{r}, t)$ is a *real* Gaussian white noise with moments satisfying the appropriate fluctuation−dissipation relation: $\langle\theta\rangle = 0, \langle\theta(\mathbf{r}, t)\theta(\mathbf{r}, t')\rangle = 2\delta(t - t')\delta(\mathbf{r} - \mathbf{r})$. In the above equations

$$\frac{\delta H[W_-, W_+]}{\delta W_-(\mathbf{r})} = C\left[\frac{2W_-}{\chi N} - \bar{\phi}_A(\mathbf{r};W_-, W_+) + \bar{\phi}_B(\mathbf{r};W_-, W_+)\right] \tag{47}$$

$$\frac{\delta H[W_-, W_+]}{\delta W_+(\mathbf{r})} = C\,[\bar{\phi}_A(\mathbf{r};\, W_-, W_+) + \bar{\phi}_B(\mathbf{r};W_-, W_+) - 1] \tag{48}$$

The evolution of the W_-^R, W_-^I and W_+^R, W_+^I fields according to the above Langevin equations (eqs 45 and 46) produces in the long-time limit the generation of field states such that the "time" averages acquire the same values as those computed using the original nonpositive-definite Boltzmann weight.[48] Equilibration of the simulation can be established by monitoring an appropriate quantity, such as the average of the imaginary component of energy/densities which should identically vanish at equilibrium. We note that with such an averaging procedure, physical observables such as the average A monomer density, $\phi_A = \langle\bar{\phi}_A\rangle$, turn out to be real, while their fluctuating analogues such as $\bar{\phi}_A$ are generally complex.

It is pertinent to note a few special features of the complex Langevin equations (eqs 45 and 46). In the absence of the noise term $\theta(\mathbf{r}, t)$, the dynamics will drive the system to the nearest saddle point. Consequently, it is straightforward to probe the stability of the mean-field solutions within the CL simulation scheme by setting the noise term identically to zero. Furthermore, this feature enables the sampling in the presence of the noise to be automatically confined near a saddle point, avoiding a long equilibration period if the system were to be prepared in an initial configuration far from the saddle point.

References and Notes

(1) Paul, D. R.; Newman, S. *Polymer Blends*; Academic Press: New York, 1978.
(2) Šolc, K., Ed.; *Polymer Compatibility and Incompatibility*; Harwood Academic Publishers: Chur, Switzerland, 1980.
(3) Flory, P. *Principles of Polymer Chemistry*; Cornell University Press: Ithaca, NY, 1971.
(4) Binder, K. *Adv. Polym. Sci.* **1994**, *112*, 181.
(5) De Gennes, P. G. *Scaling Concepts in Polymer Physics*; Cornell University Press: Ithaca, NY, 1979.
(6) Hildebrand, J. H.; Scott, R. L. *The solubility of nonelectrolytes*; Dover: New York, 1964.
(7) Bates, F. S.; Fredrickson, G. H. *Annu. Rev. Phys. Chem.* **1990**, *41*, 25. Bates, F. S. *Science* **1991**, *251*, 898.
(8) Israels, R.; Jasnow, D.; Balazs, A. C.; Guo, L.; Krausch, G.; Sokolov, J.; Rafailovich, M. *J. Chem. Phys.* **1995**, *102*, 8149.
(9) Holyst, R.; Schick, M. *J. Chem. Phys.* **1992**, *96*, 7728.
(10) Matsen, M. W.; Schick, M. *Phys. Rev. Lett.* **1994**, *72*, 2660. Matsen, M. W. *Phys. Rev. Lett.* **1995**, *74*, 4225. Matsen, M. W. *Macromolecules* **1995**, *28*, 5765. Matsen, M. W. *J. Phys.: Condens. Matt.* **2001**, *14*, R21.
(11) Jeon, H. S.; Lee, J. H.; Balsara, N. P. *Phys. Rev. Lett.* **1997** *79*, 3275. Jeon, H. S.; Lee, J. H.; Balsara, N. P. *Macromolecules* **1998**, *31*, 3328. Jeon, H. S.; Lee, J. H.; Balsara, N. P. *Macromolecules* **1998** *31*, 3340.
(12) Leibler, L. *Makromol. Chem., Macromol. Symp.* **1998**, *16*, 1.
(13) Anastasiadis, S. H.; Gancarz, I.; Koberstein, J. T. *Macromolecules* **1989**, *22*, 1449. Russell, T. P.; Anastasiadis, S. H.; Menelle, A.; Felcher, G. P.; Satija, S. K. *Macromolecules* **1991**, *24*, 1575.
(14) Lee, Y.; Char, K. *Macromolecules 27*, 2603.
(15) Pickett, G. T.; Jasnow, D.; Balazs, A. C. *Phys. Rev. Lett.* **1996**, *77*, 671.
(16) Bates, F. S.; Maurere, W. W.; Lodge, T. P.; Schulz, M. F.; Matsen, M. W.; Almdal, K.; Mortensen, K. *Phys. Rev. Lett.* **1995**, *75*, 4429.
(17) Bates, F. S.; Maurer, W. W.; Lipic, P. M.; Hillmyer, M. A.; Almdal, K.; Mortensen, K.; Fredrickson, G. H.; Lodge, T. P. *Phys. Rev. Lett.* **1997**, *79*, 849.
(18) Morkved, T. L.; Chapman, B. R.; Bates, F. S.; Lodge, T. P.; Stepanek, P.; Almdal, K. *Faraday Discuss.* **1999**, *112*, 335.
(19) Hillmyer, M. A.; Maurer, W. W.; Lodge, T. P.; Bates. F. S.; Almdal, K. *J. Phys. Chem.* **1999**, *103*, 4814.
(20) Edwards, S. F. *Proc. Phys. Soc.* **1965**, *85*, 613.
(21) Helfand, E.; Tagami, Y. *J. Polym. Sci., Part B:* **1971**, *9*, 741. Helfand, E. *J. Chem. Phys.* **1971**, *56*, 3592. Helfand, E. *J. Chem. Phys.* **1972**, *57*, 1812. Helfand, E. *J. Chem. Phys.* **1975**, *62*, 999.
(22) Scheutjens, J. M. H. M.; Fleer, G. J. *J. Chem. Phys.* **1979**, *83*, 1619.
(23) Cosgrove, T.; Vincent, B.; Scheutjens, J. M. H. M.; Fleer, G. J.; Cohen-Stuart, M. A. *Polymers at Interfaces*; Chapman and Hall: London, 1993.
(24) Noolandi, J.; Hong, K. M. *Macromolecules* **1982**, *15*, 482. Noolandi, J.; Hong, K. M. *Macromolecules* **1984**, *17*, 1531. Shi, A. C.; Noolandi, J.; Desai, R. C. *Macromolecules* **1996**, *29*, 6487.
(25) Schmid, F. *J. Phys.: Condens. Matter* **1998**, *10*, 8105.
(26) Doi M.; Edwards, S. F. *The Theory of Polymer Dynamics*; Clarendon Press: Oxford, England, 1986.
(27) Saito, N.; Takahashi, K.; Yunoki, Y. *J. Phys. Soc. Jpn.* **1967**, *219*, 22. Morse, D. C.; Fredrickson, G. H. *Phys. Rev. Lett.* **1994**, *73*, 3235.
(28) Scott, R. L. *J. Chem. Phys.* **1949**, *17*, 279.
(29) Hornreich, R. M.; Luban, M.; Shtrikman, S. *Phys. Rev. Lett.* **1975**, *35*, 1678.
(30) Broseta, D.; Fredrickson, G. H. *J. Chem. Phys.* **1990**, *93*, 2927.
(31) Naughton, J. R.; Matsen, M. W. *Macromolecules* **2002**, *35*, 8926.
(32) Leibler, L. *Macromolecules* **1980**, *13*, 1602.
(33) Fredrickson, G. H.; Helfand, E. *J. Chem. Phys.* **1987**, *87*, 697.
(34) Brazovskii, S. A. *Zh. Eksp. Teor. Fiz.* **1975**, *68*, 175. [*Sov. Phys. JETP* **1975**, *41*, 85.].
(35) Amit, D. J. *Field Theory, The Renormalization Group, and Critical Phenomena*; World Scientific: Singapore, 1984.
(36) Holden, G.; Legge, N. R.; Quirk, R. P.; Schroeder, H. E., Eds.; *Thermoplastic Elastomers*; Hanser/Garnder Publications: Cincinnati, OH, 1996.
(37) Müller, M.; Schick, M. *J. Chem. Phys.* **1996**, *105*, 8885.
(38) Werner, A.; Schmid, F.; Müller, M. *J. Chem. Phys.* **1999**, *110*, 5370.
(39) Lian, H. J.; He, X. H.; Jiang, W.; Jiang, B. Z. *Macromol. Theory Simul.* **1999**, *8*, 173.
(40) Poncela, A.; Rubio, A. M.; Freire, J. J. *J. Chem. Phys.* **2002**, *118*, 425.
(41) Kielhorn, L.; Muthukumar, M. *J. Chem. Phys.* **1998**, *110*, 4079.
(42) Kudlay, A.; Stepanow, S. *J. Chem. Phys.* **2002**, *118*, 4272.
(43) Ganesan, V.; Fredrickson, G. H. *Europhys. Lett.* **2001**, *55*, 814.
(44) Fredrickson, G. H.; Ganesan, V.; Drolet, F. *Macromolecules* **2002**, *35*, 16.
(45) Fredrickson, G. H. *J. Chem. Phys.* **2002**, *117*, 6810.
(46) Incompressibility here means that the number of monomers per volume in a given volume is constant, regardless of the size of the volume. This is possible for Gaussian chains, because they are scale invariant on small scales.
(47) Drolet, F.; Fredrickson, G. H. *Phys. Rev. Lett.* **1999**, *83*, 4317.
(48) Parisi, G. *Phys. Lett.* **1983**, *131 B*, 393.
(49) Gausterer, H. *Nucl. Phys.* **1998**, *A642*, 239.
(50) Reister, E.; Müller, M.; Binder, K. *Phys. Rev. E* **2001**, *64*. 041804.
(51) Eyert, V. *J. Comput. Phys.* **1996**, *124*, 271.
(52) Press, W. H.; Flannery, B. P.; Teukolsky, S. A.; Vetterling, W. T. *Numerical Recipes*; Cambridge University Press: Cambridge, England, 1986.
(53) Mitchell, A. R.; Griffiths, D. F. *The Finite Difference Method in Partial Differential Equations*; Wiley: Chichester, England, 1980.
(54) Feit, M. D.; Fleck, J. A.; Steiger, A. *J. Comput. Phys.* **1982**, *47*, 412.
(55) Rasmussen, K. O.; Kalosakas, G. *J. Polym. Sci.* **2002**, *B 40*, 777.
(56) Frigo, M.; Johnson, S. G. *The Fastest Fourier Transform in the West 2.1.3*; MIT: Cambridge, MA, 2000. (software package freely downloadable from www.fftw.org).
(57) Schoenmaker, W. J. *Phys. Rev. D* **1987**, *36*, 1859.
(58) The values of the correlation times depend on the details of the simulation algorithm. In simulation runs with a different ratio of $\tilde{\omega}_+$ and W_- moves, the autocorrelation times of W_-, I, and $\tilde{\omega}_+$ may become comparable. Nevertheless, our conclusion that the time scale of $\tilde{\omega}_+$ fluctuations is not coupled to that of the W_- fluctuations should remain valid, since all simulation schemes are equivalent.
(59) Düchs, D.; Schmid, F. Manuscript in preparation.
(60) Morse, D. C. *Curr. Opin. Collloid Interface Sci.* **1997**, *2*, 365.

MA030201Y